PHYSICAL REVIEW LETTERS

Inter-ELM Power Decay Length for JET and ASDEX Upgrade: Measurement and Comparison with Heuristic Drift-Based Model

T. Eich,[1,4] B. Sieglin,[1,4] A. Scarabosio,[1,4] W. Fundamenski,[2,4] R. J. Goldston,[3] A. Herrmann,[1] and ASDEX Upgrade Team[1]

[1]*Max-Planck-Institut für Plasmaphysik, EURATOM Association, Boltzmannstr 2., D-85748 Garching, Germany*
[2]*EURATOM/CCFE Association, Culham Science Centre, Abingdon, Oxon, OX14 3DB, United Kingdom*
[3]*Princeton Plasma Physics Labarotory, Princeton New Jersey 08543, USA*
[4]*JET-EFDA, Culham Science Centre, Culham, OX14 3DB, United Kingdom*

Experimental measurements of the SOL power decay length (λ_q) estimated from analysis of fully attached divertor heat load profiles from two tokamaks, JET and ASDEX Upgrade, are presented. Data was measured by means of infrared thermography. An empirical scaling reveals parametric dependency λ_q in mm $= 0.73 B_T^{-0.78} q_{\mathrm{cyl}}^{1.2} P_{\mathrm{SOL}}^{0.1} R_{\mathrm{geo}}^0$, where $B_T(T)$ describes the toroidal magnetic field, q_{cyl} the cylindrical safety factor, $P_{\mathrm{SOL}}(MW)$ the power crossing the separatrix and $R_{\mathrm{geo}}(m)$ the major radius of the device. A comparison of these measurements to a heuristic particle drift-based model shows satisfactory agreement in both absolute magnitude and scaling. Extrapolation to ITER gives $\lambda_q \simeq 1$ mm.

I. Introduction.—Operation in diverted high confinement mode (H mode [1]) is the foreseen scenario for next step tokamak fusion devices. H-mode plasmas develop an edge transport barrier close to the magnetic boundary separating the closed-field-line region from the open-field-line region or scrape-off layer (SOL). Operation in H mode is accompanied by periodic relaxation phenomena called edge-localized modes (ELMs) [2]. The power decay length, λ_q, in the SOL region is a crucial quantity concerning the divertor peak heat load ($q_{\max}$) for current and future devices. Despite the importance of an accurate prediction of λ_q, a commonly accepted theoretical model or empirical extrapolations from current devices to ITER remain elusive. Such an attempt must include at least two devices with different linear dimensions to establish a major radius dependency, as done in this work where data from ASDEX Upgrade (AUG) and JET are used.

Infrared camera systems with a target resolution of 1.7 mm and framing rates of about 10 kHz are employed. Energy effluxes due to ELMs [3] are observed to impose toroidally asymmetric heat flux (q) patterns on the divertor target [4–6] and larger power decay lengths [7]. Additionally as shown in Fig. 1, radial movements of the strike line on target, with amplitudes reaching up to the power decay length itself, are observed in JET plasma discharges modulated by ELM induced energy and particle losses [8]. The same phenomenology is observed in AUG. Taking both effects together, ELM averaged estimates of λ_q give too large absolute numbers and different parameter dependency [9]. Thus, to reach improved accuracy, inter-ELM periods from 90% to 99% of the ELM cycle time are defined, removing any influences from the latter effects. The heat flux between ELMs and that during ELMs are due to different physical processes. Only by examining them separately can the processes be understood and scaled to

future devices. This Letter analyses the inter-ELM heat fluxes.

The data base covers 56 and 11 deuterium type-I ELMy H-mode plasmas for JET and AUG, respectively, summarised in Table I. We denote plasma current as I_p,
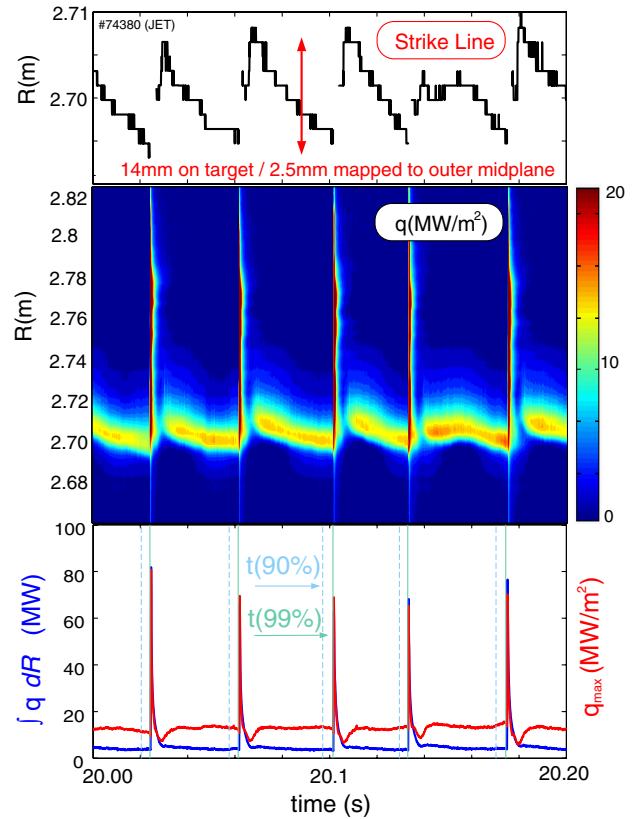

FIG. 1 (color online). Evolution of heat flux and the inferred strike line position on the divertor target for a typical JET discharge.

TABLE I.   Database of analyzed discharges.

	I_p [MA]	B_T [T]	q_{95}	P_h [MW]	δ	Z_{eff}	n_{GW}
JET	1.0–3.5	1.1–3.2	2.6–5.5	5–24	0.2–0.4	1.5–2.5	0.4–0.8
AUG	0.8–0.9	2.0–2.4	4.5–5.1	3–13	0.2–0.4	2.0–2.7	0.5–0.7

toroidal magnetic field as B_T, edge safety factor as q_{95}, heating power as P_h, averaged triangularity as δ, effective charge as Z_{eff} and Greenwald density fraction as n_{GW}. The aspect ratio of both machines, defined as $\epsilon = a/R_{geo}$, is $\epsilon = 0.32$, with the major geometrical radius denoted as R_{geo} and the minor radius as a. The plasma elongation amounts to $\kappa = 1.8$ for both devices. Heat flux profiles are analyzed with minimal gas puffing and in the absence of power detachment with carbon divertor plasma-facing components.

II. Experimental estimation of the power decay length.— The SOL power decay length is determined by analysis of heat flux profiles measured on the outer divertor target by means of infrared thermography. Details of the experimental setup for JET can be found in Ref. [7] and for AUG in Ref. [10]. In order to relate the surface heat flux profile to the outer midplane separatrix region, the magnetic flux expansion, f_x, has to be taken into account. We use the definition for an integral flux expansion along the target surface [10,11] calculated for the outer midplane region $R = R_{sep}$ to $R = R_{sep} + 5$ mm, with R_{sep} being the outer separatrix radius. The variation of f_x by using $R = R_{sep} + 2.5$ mm amounts to <5%.

By expressing the target coordinate as s and the strike line position on target as s_0 we describe the heat load profile at the divertor entrance as

$$q(\bar{s}) = q_0 \exp\left(-\frac{\bar{s}}{\lambda_q f_x}\right) \quad \text{and} \quad \bar{s} = s - s_0, \qquad s \geq s_0$$

(1)

This simple ansatz allows to account for perpendicular heat diffusion or *leakage* into the private-flux-region (PFR) by introducing a Gaussian width S representing the competition between parallel and perpendicular heat transport in the divertor volume. This means that, physically, the exponential profile at the divertor entrance [12], is diffused into the private flux region while travelling towards the target [13]. This competition is approximated by a convolution of the exponential profile with a Gaussian function with the width S [14]. The target heat flux profiles are thus expressed as ($s \in [-\infty, \infty]$)

$$q(\bar{s}) = \frac{q_0}{2} \exp\left[\left(\frac{S}{2\lambda_q f_x}\right)^2 - \frac{\bar{s}}{\lambda_q f_x}\right] \text{erfc}\left(\frac{S}{2\lambda_q f_x} - \frac{\bar{s}}{S}\right) + q_{BG}$$

(2)

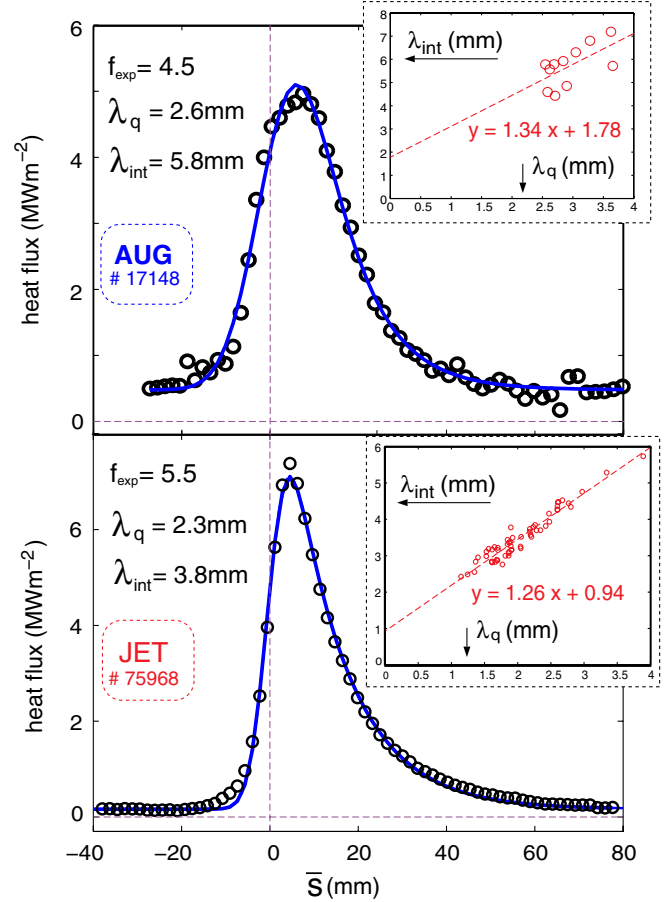Figure 2 shows examples for measured heat flux profiles and fitting results by using Eq. (2) with the free constant

FIG. 2 (color online).   Heat flux profiles measured on the outer divertor target and fits using Eq. (2). The inserts show the relation between λ_q and λ_{int} which are well expressed by a linear fit.

parameters S, λ_q, q_0, q_{BG} and s_0. Two-dimensional numerical heat diffusion calculations [15] using Spitzer-like ($\propto T^{5/2}$) parallel and Bohm-like perpendicular ($\propto T$) thermal diffusivities show that this technique is accurate to better than 6.5% in determining λ_q at the divertor entrance in cases where the deduced Gaussian width (S) is less than 70% of the exponential width, which is the case for the complete data base. For the mean value of all presented data we get $S/\lambda_q = 0.42$ corresponding to 2% accuracy. Typical values of the field line target inclination angle at $\bar{s} = 0$ are in JET $\simeq 3°$ and in AUG $\simeq 4°$ and relative changes from $\bar{s} = 0$ to $\bar{s} = \lambda_q f_x$ are between 2% and 14% for both devices.

From Eq. (2) follows the integral power decay width [11]

$$\lambda_{int} = \frac{\int [q(s) - q_{BG}] ds}{q_{max}} f_x^{-1}$$

(3)

This quantity is frequently used in the literature [11] since it allows to relate the peak heat load on the divertor target to power deposited on the divertor target, a crucial design

parameter for the power handling capabilities of a large device such as ITER. The relation between exponential and integral decay lengths for JET and AUG is found by linear least squares fitting to be

$$\lambda_{\text{int}}^{\text{JET}} = 1.26\lambda_q^{\text{JET}} + (0.94 \pm 0.32) \text{ mm}$$
$$\lambda_{\text{int}}^{\text{AUG}} = 1.34\lambda_q^{\text{AUG}} + (1.78 \pm 0.68) \text{ mm} \qquad (4)$$

revealing that λ_q is not a constant fraction of λ_{int} as assumed in earlier studies using simple exponential fit of the SOL part of the heat flux profile [11]. The resulting λ_{int} from Eq. (2) can be viewed as due to the combination of an exponential profile or parallel heat flux near the plasma, with further radial diffusion both into the PFR and SOL on the divertor side of the x point. This latter is expected to vary with the divertor geometry, and so would not necessarily be well parametrized by global plasma parameters.

III. Multiparameter regression.—We provide here empirical regressions for λ_q for JET and for the combined data set from JET and AUG deuterium discharges. A regression for AUG only is not attempted, due to the small variations in I_p and B_T. The regression parameters are B_T, cylindrical safety factor (q_{cyl}), power crossing the separatrix (P_{SOL}) and R_{geo} when regressing combined data from both devices. The cylindrical safety factor is expressed by

$$q_{\text{cyl}} = \frac{2\pi a \epsilon B_T}{\mu_0 I_p} \frac{(1 + \kappa^2)}{2}. \qquad (5)$$

The aspect ratio and elongation of both devices are identical and hence cannot be regressed. We apply least square fitting to derive a parametric dependency

$$\lambda \text{ (mm)} = C_0[B_T^{C_B} \text{ (T)}]q_{\text{cyl}}^{C_q}[P_{\text{SOL}}^{C_P} \text{ (MW)}][R_{\text{geo}}^{C_R} \text{ (m)}]. \qquad (6)$$

Results are summarized in Table II for λ_q and λ_{int} including the regression variances for each variable. For completeness we note that regressions with q_{95} and q_{cyl} give identical dependencies within the error bars. Here we point on the main finding that λ_q has a strong dependency on B_T and q_{cyl}, minor dependency on P_{SOL}. Notably no dependency of λ_q on R_{geo} is detected.

TABLE II. Parameter dependency of λ_q and λ_{int}.

		C_0	C_B	C_q	C_P	C_R
JET	λ_q	0.70	−0.84	1.23	0.14	⋯
	±	0.26	0.26	0.26	0.14	⋯
JET+	λ_q	0.73	−0.78	1.20	0.10	0.02
AUG	±	0.38	0.25	0.27	0.11	0.20
JET	λ_{int}	1.49	−0.66	0.93	0.13	⋯
	±	0.43	0.19	0.19	0.11	⋯
JET+	λ_{int}	3.19	−0.47	0.82	−0.05	−0.39
AUG	±	1.49	0.21	0.25	0.09	0.18

IV. Comparison to heuristic drift-based model.—Recently a heuristic model has been introduced [16], predicting the absolute value and scaling of the power scrape-off width in H-mode tokamak plasmas. Favorable qualitative comparison with results from a number of experiments was shown. Here we provide a more stringent test of this model against the data base developed from JET and AUG. The model assumes that parallel plasma flow velocity amounts to $c_s/2$ with c_s being the ion sound speed. This sets the particle residence time in the scrape-off layer. The scrape-off layer width is found by multiplying this residence time with the grad B and curvature electron drift velocity. The edge temperature, which determines the drift speed, is found by balancing Spitzer parallel thermal conduction along field lines with the heat flux across the field line. The resulting power fall-off length is given by

$$\lambda_m = 2.02 \frac{f_{\text{AZ}}}{\sqrt{(1 + \kappa^2)}\epsilon^{1/8}} B_T^{-7/8} q_{\text{cyl}}^{9/8} P_{\text{SOL}}^{1/8} \qquad (7)$$

with λ_m in [mm], P_{SOL} in [MW], B_T in [T] and

$$f_{\text{AZ}} = \left(\frac{2\bar{A}}{1 + \bar{Z}}\right)^{7/16}\left(\frac{Z_{\text{eff}} + 4}{5}\right)^{1/8}$$
$$\bar{Z} = \sum_i Z_i n_i / \sum_i n_i, \qquad (8)$$
$$\bar{A} = \sum_i n_i A_i / \sum_i n_i.$$

The values for $\bar{A}$ and $\bar{Z}$ are calculated by assuming carbon to be the dominant impurity. The charge state distribution of carbon is taken from Ref. [17] by assuming 100 eV for the separatrix temperature [18].

The drift-based model result shown in Eq. (7) represents the mean width of the power scrape-off width poloidally around the plasma, which follows the poloidal flux. Since the JET and AUG results are mapped to the outer midplane, it is appropriate to map λ_m to the outer midplane

$$\lambda_m^* = \frac{R_{\text{geo}}}{(R_{\text{geo}} + a)} \frac{B_p}{B_p^{mp}} \lambda_m \qquad (9)$$

with

$$B_p = \frac{\mu_0 I_p}{2\pi a\sqrt{(1 + \kappa^2)/2}}, \qquad (10)$$

and where B_p^{mp} describes the poloidal magnetic field at the outer midplane region. For the data base we find in average $\lambda_m^* = (0.55 \pm 0.05)\lambda_m$.

Figure 3 shows the comparison of experimental data with the model prediction, complemented by adding 10 helium and 7 hydrogen discharges for JET. Error bars are due to uncertainties in P_{SOL}, Z_{eff}, carbon charge distribution [17], plasma purity, and experimental estimation of λ_q. To compare the model prediction to the regression results for deuterium discharges from JET and AUG we use $Z_{\text{eff}} = 2$, $\kappa = 1.8$, $\epsilon = 0.32$. As shown in Table III,
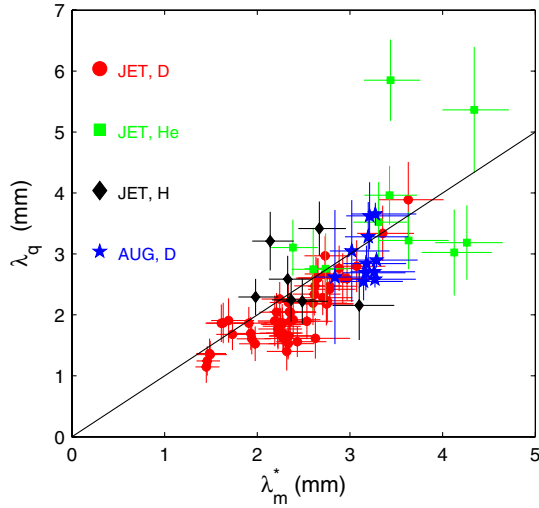
FIG. 3 (color online).   Comparison of predicted λ_m^* to experimental λ_q for deuterium (D), hydrogen (H), helium (He) plasmas.

TABLE III.   Summary of regression and model prediction.

	C_0	C_B	C_q	C_P	C_R
λ_m^*	0.92	-0.875	1.125	0.125	0
λ_q	0.73 ± 0.38	-0.78 ± 0.25	1.20 ± 0.27	0.10 ± 0.11	0.02 ± 0.20

agreement with both absolute magnitude and scaling dependency is found.

V. Conclusions.—An approximative expression for the target heat load profiles is introduced. From this expression we are enabled to derive λ_q in addition to λ_{int}. A most notable conclusion of the analysis of λ_q is that no machine size scaling is detected which has important impact on future larger machines. As shown in Fig. 3, typical numbers for λ_q in JET are smaller than in AUG mainly due to the higher q_{95} (or q_{cyl}). Given the similar q_{95} (or q_{cyl}) value and higher toroidal magnetic field in next step devices such as ITER, smaller values for λ_q have to be expected for non detached divertor plasma conditions, when compared with JET. The design values for ITER of interest here are $R = 6.2$ m, $a = 2.0$ m, $\kappa = 1.7$, $P_{SOL} = 120$ MW, $B_{tor} = 5.3$ T, $I_p = 15$ MA, $q_{cyl} = 2.42$, $Z_{eff} = 1.6$. Extrapolation and model predict for deuterium plasmas $\lambda_q^{ITER} = 0.94$ mm and $\lambda_q^{ITER} = 0.97$ mm, respectively.

Extrapolation of λ_{int} to ITER cannot be given from this work. Assuming that the offset (which is related to the S parameter) between λ_q and λ_{int} in ITER is similar to JET and AUG, we find for ITER $\lambda_{int} = 1.3\lambda_q + (1.36 \pm 0.43$ mm$) \simeq 2.6 \pm 0.4$ mm. The latter value is close to the lower range of the values predicted in Ref. [19]. However employing a direct extrapolation to ITER from the scaling in Table II we find $\lambda_{int} \simeq 1.2$ mm. This is a direct result of the negative size dependence of λ_{int} caused by different offsets observed in Eq. (4) which are in turn due to the variations of the divertor geometry. The long, baffled divertor in the ITER design may result in larger values of S than observed on AUG or JET. Only dedicated experiments aiming to find a scaling of S, can lead to a better understanding here.

The comparison of JET and AUG power fall-off length (λ_q) for deuterium type-I ELMy H-Modes to the heuristic model prediction [16] of the power scrape-off width, based on parallel convection and curvature drifts, is satisfactory with regard to both magnitude and scaling, and may provide a reasonable baseline for the experimental study of techniques to increase this width.

ITER is anticipated to operate in conditions with a high fraction of SOL radiation and partially detached divertor plasmas, unlike the conditions studied here, but the current assumption [20] that λ_q will be in the range of 5 mm, when attached conditions are encountered, needs to be revisited.

[1] F. Wagner *et al.*, Phys. Rev. Lett. **49**, 1408 (1982).
[2] D. N. Hill, J. Nucl. Mater. **241–243**, 182 (1997).
[3] A. Loarte *et al.*, J. Nucl. Mater. **313–316**, 962 (2003).
[4] T. Eich, A. Herrmann, and J. Neuhauser, Phys. Rev. Lett. **91**, 195003 (2003).
[5] S. Devaux *et al.*, J. Nucl. Mater. **415**, S865 (2011).
[6] A. Wingen, T. E. Evans, C. J. Lasnier, and K. H. Spatschek, Phys. Rev. Lett. **104**, 175001 (2010).
[7] T. Eich *et al.*, J. Nucl. Mater. **415**, S856 (2011).
[8] E. Solano *et al.*, Nucl. Fusion **48**, 065005 (2008).
[9] W. Fundamenski *et al.*, Nucl. Fusion **45**, 950 (2005).
[10] A. Herrmann *et al.*, Plasma Phys. Controlled Fusion **44**, 883 (2002).
[11] A. Loarte *et al.*, J. Nucl. Mater. **266–269**, 587 (1999).
[12] P. Stangeby *et al.*, Nucl. Fusion **50**, 125003 (2010).
[13] A. Loarte *et al.*, Contrib. Plasma Phys. **32**, 468 (1992).
[14] F. Wagner, Nucl. Fusion **25**, 525 (1985).
[15] R. Goldston, Phys. Plasmas **17**, 012503 (2010).
[16] R. Goldston, *38th EPS Conference on Controlled Fusion and Plasma Physics* (European Physical Society, Strasbourg, France, 2011), P1.074.
[17] T. Pütterich *et al.*, J. Nucl. Mater. **415**, S334 (2011).
[18] A. Kallenbach *et al.*, Plasma Phys. Controlled Fusion **46**, 431 (2004).
[19] W. Fundamenski *et al.*, Nucl. Fusion **51**, 083028 (2011).
[20] (ITER Phys. Exp. Group), Nucl. Fusion **47**, S203 (2007).
[21] F. Romanelli *et al.*, Nucl. Fusion **51**, 094008 (2011). (All the members of the JET-EFDA Collaboration appear in the appendix of this Letter.)